Journal of Solid State Chemistry 183 (2010) 379–384

Contents lists available at ScienceDirect

Journal of Solid State Chemistry

journal homepage: www.elsevier.com/locate/jssc

Structural refinement of $T_2Mo_3O_8$ (T=Mg, Co, Zn and Mn) and anomalous valence of trinuclear molybdenum clusters in $Mn_2Mo_3O_8$

Hideki Abe *, Akira Sato, Naohito Tsujii, Takao Furubayashi, Masahiko Shimoda

National Institute for Materials Science (NIMS), Sengen 1-2-1, Tsukuba, Ibaraki 305-0047, Japan

ARTICLE INFO

Article history:
Received 6 August 2009
Received in revised form
4 November 2009
Accepted 21 November 2009
Available online 29 December 2009

Keywords:
Mo
Trinuclear cluster
Valence
Non-bonding molecular orbital
Unpaired electron

ABSTRACT

Crystal structure of a series of mixed-metal oxides, $T_2Mo_3O_8$ (T=Mg, Co, Zn and Mn; $P6_3mc$; a=5.7628(1) Å, c=9.8770(3) Å for $Mg_2Mo_3O_8$; a=5.7693(3) Å, c=9.9070(7) Å for $Co_2Mo_3O_8$; a=5.7835(2) Å, c=9.8996(5) Å for $Zn_2Mo_3O_8$; a=5.8003(2) Å, c=10.2425(5) Å for $Mn_2Mo_3O_8$) was investigated by X-ray diffraction on single crystals. Structural analysis, magnetization measurements, X-ray photoemission spectroscopy and cyclic voltammetry showed that the Mn ions at the tetrahedral and octahedral sites in $Mn_2Mo_3O_8$ adopt different valences of +2 and $2+\delta$ ($\delta>0$), respectively. The formal valence of the Mo_3 in $Mn_2Mo_3O_8$ is $12-\delta$ to retain electric neutrality of the compound. In contrast, the T ions and Mo_3 in $T_2Mo_3O_8$ (T=Mg, Co and Zn) adopt the valences of +2 and +12, respectively.

1. Introduction

Inorganic compounds containing transition-metal clusters are of growing importance as catalysts for the synthesis of organic materials [1]. A carbonyl complex of trinuclear ruthenium, $[Ru_3(\mu_3\text{-ampy})(\mu\text{-}\eta^1\text{:}\eta^2\text{-PhC=CHPh})(CO)_8]$ (Hampy=2-amino-6-methylpyridine), catalyzes the selective hydrogenation of diphenylacetylene [2]. $[Ru_3(\mu_3,\eta^2,\eta^3,\eta^5\text{-acenaphthylene})(CO)_8]$ is a good catalyst towards the reaction of secondary amides with hydrosilanes [3]. Unlike Ru_3, the trinuclear cluster of tetravalent molybdenum, $Mo^{4+}{}_3{}^{12+}$, does not act as an effective catalysis center. A sulfo-complex of Mo_3^{12+}, $[Mo_3^{12+}Cu^+S_4(dmpe)_3Cl_4]^+$ (dmpe=1,2-bis(dimethylphosphino)ethane), exceptionally catalyzes organic reactions including the intramolecular cyclization of diazo ketones and/or the intermolecular cyclopropanation of styrene with ethyl diazo acetate [4,5]. The catalytic activity of $[Mo_3^{12+}Cu^+S_4(dmpe)_3Cl_4]^+$ is, however, solely ascribed to Cu^+ instead of Mo_3^{12+} [5].

The catalytic inertness of Mo_3^{12+} is explained on the basis of the Hückel theory [6,7]. A Mo_3 cluster incorporated in inorganic compounds is described as an isolated molecule with molecular orbitals consisting of Mo 4*d* orbitals. The bonding molecular orbitals of Mo_3^{12+} are fully occupied to form a stable closed shell that is catalytically inert [7]. This theoretical picture is consistent with the fact that the most usual valence of Mo_3 is +12 for the known Mo_3-containing complexes, excluding few compounds in which Mo_3 adopts +11 [8]. It is of practical interest if Mo_3 can adopt a valence other than +12 to become catalytically active, when it is incorporated in a structural framework other than that of molecular complexes [9,10].

We have focused on a series of mixed-metal oxides that incorporate Mo_3 in the solid-state framework, $T_2Mo_3O_8$ (T=Mg, Zn, Mn, Fe, Co, Ni or Cd) [11–24]. Fig. 1a shows a [001] view of the crystal structure of $T_2Mo_3O_8$. Thirteen oxygen atoms are coordinated to a Mo_3 to construct a larger unit of $[Mo_3O_{13}]$ (Fig. 1a, depicted by a ball-and-stick model). The $[Mo_3O_{13}]$ units share the oxygen atoms at the O2 and O3 sites to form two-dimensional Mo_3O_8 layers (Figs. 1a and b, represented by dark gray polygons). Two adjacent Mo_3O_8 layers sandwich T ions that are either tetrahedrally (Fig. 1b; T1 sites, represented by light gray tetrahedra) or octahedrally (Figs. 1a and b; T2 sites, represented by light gray octahedra) coordinated by oxygen atoms. To date, the valences of the T ions and Mo_3 in $T_2Mo_3O_8$ have been presumed to be +2 and +12, respectively [11–24].

On the basis of X-ray diffractometry (XRD) on single crystals, magnetization measurements, X-ray photoemission spectroscopy (XPS) and cyclic voltammetry, we demonstrate that the Mo_3 in $Mn_2Mo_3O_8$ adopt an anomalous valence of $12-\delta$ ($\delta>0$) instead of +12. The valences of the Mn ions at the T1 and T2 sites in $Mn_2Mo_3O_8$ are +2 and $2+\delta$, respectively, which retains electric neutrality of the compound. In contrast to $Mn_2Mo_3O_8$, the valences of the T ions and Mo_3 in $T_2Mo_3O_8$ (T=Mg, Co or Zn) are +2 and +12, respectively. The $Mo_3^{12-\delta}$ in $Mn_2Mo_3O_8$ has excessive electrons relative to Mo_3^{12+}. The excessive electrons are most

* Corresponding author. Fax: +81 29 859 2301.
E-mail address: ABE.hideki@nims.go.jp (H. Abe).

0022-4596/$ - see front matter © 2009 Elsevier Inc. All rights reserved.
doi:10.1016/j.jssc.2009.11.024

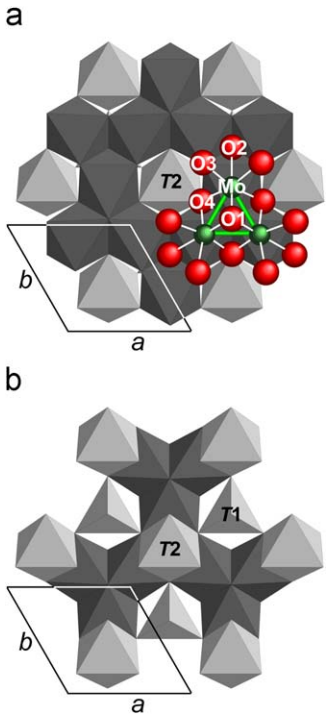

Fig. 1. Crystal structure of $T_2Mo_3O_8$, viewed from the [001] direction, together with the unit cell. (a) Mo_3O_8 layer (dark gray polygons), together with $T2O_6$ octahedra (light gray). A $[Mo_3O_{11}]$ unit is depicted by a ball-and-stick model. (b) Configuration of the $T1$ (light gray tetrahedra) and $T2$ sites beneath the Mo_3O_8 layer of Fig. 1a.

likely accepted by a non-bonding molecular orbital of $Mo_3^{12-\delta}$ to be unpaired electrons. Unlike any known Mo_3^{12+}-containing compounds, $Mn_2Mo_3O_8$ has potential as a Lewis-base catalyst, due to the unpaired electron on the $Mo_3^{12-\delta}$.

2. Material and methods

2.1. Sample preparation

Single crystals of $T_2Mo_3O_8$ (T=Mg [18], Co [18], Zn [18] and Mn) were synthesized by electrolysis of molten molybdates that dissolved the T ions of the desired compounds. The electrolyte for $Mg_2Mo_3O_8$ was a 1:1 mole mixture of Cs_2MoO_4 (99% purity, Soekawa Chemical) and $MgMoO_4$ (99.9% purity, Soekawa Chemical). The electrolyte for $Co_2Mo_3O_8$ was a 1:1:1 mole mixture of Cs_2MoO_4, CoO (99% purity, Koso Chemical) and MoO_3 (99.9% purity, Mitsuwa Chemical). The electrolyte for $Zn_2Mo_3O_8$ was a 1:1:1 mole mixture of Cs_2MoO_4, ZnO (99.99% purity, Kojundo Kagaku) and MoO_3. The electrolyte for $Mn_2Mo_3O_8$ was a 1:1:1 mole mixture of Cs_2MoO_4, $Mn(CO_3)$ $0.5H_2O$ (Kishida Chemical) and MoO_3. The net weight of the electrolytes was 4.0 g for any $T_2Mo_3O_8$.

Alumina boats $10 \times 10 \times 100\,mm^3$ in width, depth, and length, respectively, were used as electrolyte containers. Working and counter electrodes (Pt wires with a diameter of 1 mm) were fixed at the opposite ends of an electrolyte container. A reference electrode (a Pt wire with a diameter of 1 mm) was fixed near the working electrode. All the electrodes were connected to a potentiostat (Hokuto Denko, Model HA-151) with Pt leads having a diameter of 0.3 mm. The electrolyte container, equipped with Pt electrodes, was filled with the electrolyte for the desired $T_2Mo_3O_8$. The electrolyte was molten by heating in air up to 1050 °C. The melt was electrolyzed over 1 h at a constant current of 20 mA. The electrolysis was terminated by removing the electrodes from the melt. Black hexagonal crystals of $T_2Mo_3O_8$ precipitated at the tip of the working electrode. The average size of the crystals was 0.5 mm^3, regardless of the kind of T ion. The crystals were washed by soaking overnight in an aqueous solution that dissolved 1 $g\,l^{-1}$ each of ethylene diamine tetraamino acid (EDTA; 99.5% purity, Kishida Chemical) and $NaHCO_3$ (99% purity, Kishida Chemical).

2.2. Characterization

Powder X-ray diffraction (pXRD; RIGAKU RINT 2000, Cu$K\alpha$ radiation, λ=1.541 Å) was performed on the powdered crystals of $T_2Mo_3O_8$. Single-crystal XRD was performed with graphite-monochromatized Mo$K\alpha$ radiation (λ=0.71073 Å), using a Bruker SMART APEX CCD area-detector diffractometer. Magnetization measurements were performed with a superconductive quantum interference device (SQUID) magnetometer (MPMS, Quantum Design) at a magnetic field of 1 T in a temperature range from 2 to 800 K. Quartz tubes were used as sample holders for magnetic measurements. Magnetization of empty sample holders was subtracted from the magnetization of the specimens.

X-ray photoemission spectroscopy (XPS) measurements were performed at room temperature in an ultra-high vacuum using a VG ESCALAB MkII spectrometer and Al-α radiation (1487 eV). The reference specimens, MnO, Mn_2O_3 and MnO_2 (all 99% purity, Kishida Chemical), were used as purchased. Specimens for XPS measurements were prepared by mixing the powdered crystals of $T_2Mo_3O_8$ and/or the reference specimens with carbon black. The XPS data were referenced to the C 1s emission (284.5 eV) of the adventitious carbon black as an internal standard. The XPS spectra were fitted using mixed Gaussian–Lorentzian functions.

Cyclic voltammetry (CV) measurements were performed in the same electrolytes as those for the synthesis of $T_2Mo_3O_8$: a 1:1 mole mixture of Cs_2MoO_4 and $MgMoO_4$ for $Mg_2Mo_3O_8$; a 1:1:1 mole mixture of Cs_2MoO_4, CoO and MoO_3 for $Co_2Mo_3O_8$; a 1:1:1 mole mixture of Cs_2MoO_4, ZnO and MoO_3 for $Zn_2Mo_3O_8$; a 1:1:1 mole mixture of Cs_2MoO_4, $Mn(CO_3)$ $0.5H_2O$ and MoO_3 for $Mn_2Mo_3O_8$. CV measurements were performed in air at 1050 °C. The sweep rate for CV measurements was 10 $mV\,s^{-1}$. Pt wires with a diameter of 1 mm were used as the working and counter electrodes. The electrode potentials for CV measurements were referenced to a Pt wire electrode with a diameter of 1 mm.

3. Results and discussion

Fig. 2 shows pXRD profiles for $T_2Mo_3O_8$, together with a pattern simulated using the following crystallographic parameters: $P6_3mc$; a=5.8 Å and c=9.9 Å. The pXRD profiles of $Mg_2Mo_3O_8$, $Co_2Mo_3O_8$ and $Zn_2Mo_3O_8$ are consistent with the simulated pattern, excluding the impurity peaks of MgO and CoO for $Mg_2Mo_3O_8$ and $Co_2Mo_3O_8$, respectively. The pXRD profile for $Mn_2Mo_3O_8$ shows a significant shift to lower angles relative to the simulation.

The inset shows the lattice parameters of $T_2Mo_3O_8$, calculated from the peak positions of the pXRD profiles, as functions of the ionic radius (I_r) of the T ions. The values of I_r are based on the premise that the T ions are divalent and octahedrally coordinated by oxygen atoms: Mg^{2+} (I_r=0.66 Å), Co^{2+} (I_r=0.72 Å), Zn^{2+} (I_r=0.74 Å) and Mn^{2+} (I_r=0.80 Å) [25]. The a-parameter of $T_2Mo_3O_8$ slightly increases with the increase in I_r. The c-parameter also tends to increase up to I_r=0.74 Å (Zn^{2+}). When I_r=0.80 Å (Mn^{2+}), the c-parameter abruptly increases by 3.4 percents relative to the value at I_r=0.74 Å (Zn^{2+}). The low-angle shift of the pXRD profile for $Mn_2Mo_3O_8$ relative to those for the

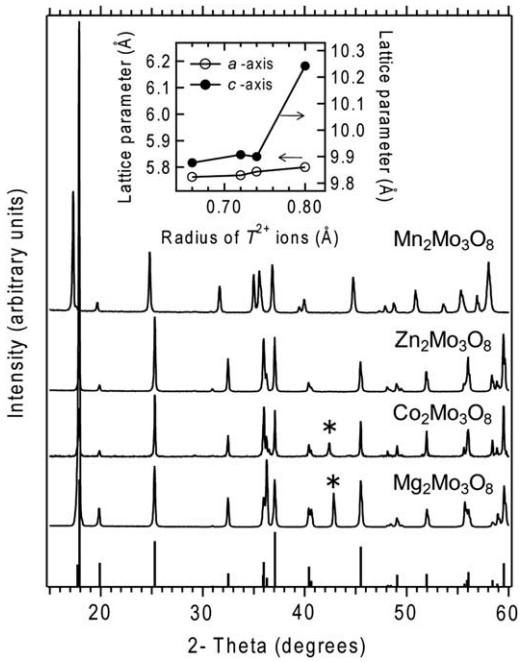

Fig. 2. *p*XRD profiles for $T_2Mo_3O_8$ (T=Mg, Co, Zn and Mn). Inset shows the relation between the ionic radius of the T^{2+} ions and the lattice parameters of $T_2Mo_3O_8$. Asterisked peaks in the profiles of $Mg_2Mo_3O_8$ and $Co_2Mo_3O_8$ are assigned to MgO and CoO, respectively.

Table 1
Crystallographic data for $T_2Mo_3O_8$.

Formula	$Mg_2Mo_3O_8$	$Co_2Mo_3O_8$	$Zn_2Mo_3O_8$	$Mn_2Mo_3O_8$
Formula weight	464.44	533.68	546.56	525.70
Crystal system	Hexagonal	Hexagonal	Hexagonal	Hexagonal
Space group	$P6_3mc$	$P6_3mc$	$P6_3mc$	$P6_3mc$
a (Å)	5.7628(1)	5.7693(3)	5.7835(2)	5.8003(2)
c (Å)	9.8770(3)	9.9070(7)	9.8996(5)	10.2425(5)
V (Å^3)	284.068(11)	285.57(3)	286.77(2)	298.43(2)
Z	2	2	2	2
Temperature (K)	293	293	293	293
μ (Mo$K\alpha$) (mm^{-1})	6.601	12.10	14.63	10.25
2θ range (deg)	0–105	0–80.82	0–82.21	0–80.64
Reflections collected	8266	4685	4723	4901
Unique reflections	1201	730	741	724
R_{int}	0.0413	0.0309	0.0398	0.0350
$R1$ ($F_0 > 4\ \sigma\ (F_0)$)[a]	0.0271	0.0186	0.0267	0.0352
$R1$ on all data[a]	0.0275	0.0189	0.0270	0.0355
$wR2$ on all data[b]	0.0637	0.0444	0.0673	0.0859
Refined parameters	32	31	31	31
Residual peaks, eÅ^{-3}	0.46	0.22	0.23	0.58

[a] $R1 = \Sigma||F_0| - |F_c||/\Sigma|F_0|$.
[b] $wR2 = (\Sigma[w(F_0^2 - F_c^2)^2]/\Sigma[wF_0^4])^{1/2}$.

other $T_2Mo_3O_8$ (T=Mg, Co or Zn) is, therefore, ascribed to the exceptionally large c-parameter of $Mn_2Mo_3O_8$.

Single-crystal XRD was performed to obtain more detailed structural information. The crystal structures were refined on the basis of literature, using the SHELXL97 program (Table 1) [11–13,16]. The refined positional parameters, isotropic equivalent atomic displacement parameters and site occupancy factors are provided as supporting information, together with literature values (S1). The refined positional parameters for $T_2Mo_3O_8$ (T=Mg and Zn) are consistent with the literature [11–13,16].

The interatomic distances for $T_2Mo_3O_8$ were calculated using the crystallographic data as well as the refined positional parameters (Table 2). The T–O distances, calculated using literature values for the ionic radii of oxygen and of the T ions (Mg^{2+}, Co^{2+}, Zn^{2+}, Mn^{2+} and Mn^{3+}), are also presented in parentheses [25]. The calculated T–O distances for the T ions=Mg^{2+}, Co^{2+}, Zn^{2+}, are consistent with the observed values. The calculated value for the T ion=Mn^{2+} is consistent with the observed Mn2–O3 distance, but shows a considerable deviation from the observed Mn2–O4 distance. Instead, the observed Mn2–O4 distance is consistent with the value calculated for the T ion=Mn^{3+}. The interatomic distances of the neighboring Mo atoms in Mo_3 clusters are less dependent on the kind of the T ions than the T–O distances. It is worth noting, however, that the Mo–Mo distance for $Mn_2Mo_3O_8$ is larger by 0.3% than the value for $Zn_2Mo_3O_8$ and by 0.5% than the values for $Mg_2Mo_3O_8$ or $Co_2Mo_3O_8$.

The bond valences of the T ions in $T_2Mo_3O_8$, V_T, were calculated using the equation, $V_T = \Sigma \exp((R_0 - \text{the observed } T\text{–O distance})/0.370)$ (Table 3) [26]. The calculated bond valences for T=Mg, Co and Zn are, regardless of site, consistent with the value expected for divalent ions, +2. The bond valence calculated for Mn1 is also consistent with +2. The bond valence calculated for Mn2 shows, however, a considerable deviation from +2 by 13%. The analysis on the T–O distances and/or the bond valences suggests that the Mn2 ions in $Mn_2Mo_3O_8$ adopt a higher valence than +2. The calculated bond valences of Mo in $T_2Mo_3O_8$ are also listed in Table 3. The bond valences of Mo for $Zn_2Mo_3O_8$ (+3.999) and $Mn_2Mo_3O_8$ (+4.007) are slightly smaller than those for $Mg_2Mo_3O_8$ (+4.054) or $Co_2Mo_3O_8$ (+4.060).

Fig. 3 shows magnetic susceptibilities of $T_2Mo_3O_8$ as functions of temperature. The green squares and red hatches represent the magnetic susceptibilities of $Mg_2Mo_3O_8$ (χ_{Mg}) and $Zn_2Mo_3O_8$ (χ_{Zn}), respectively. Both χ_{Mg} and χ_{Zn} are virtually independent of temperature from 50 to 300 K. The amplitudes of both χ_{Mg} and χ_{Zn} are very small ($< 1 \times 10^{-3}$ emu mol^{-1}) over the whole temperature range. The non-magnetic behavior of $Mg_2Mo_3O_8$

Table 2
X-ray interatomic distances for $T_2Mo_3O_8$.

	Distances (Å)			
	$Mg_2Mo_3O_8$	$Co_2Mo_3O_8$	$Zn_2Mo_3O_8$	$Mn_2Mo_3O_8$
$T1$–O2	1.951(3) (1.99)	1.947(4) (–)	1.947(7) (2.00)	2.012(7) (–)
$T1$–O3	1.9545(17) (1.99)	1.966(3) (–)	1.963(4) (2.00)	2.032(5) (–)
$T2$–O3	2.101(2) (2.12)	2.122(3) (2.14)	2.128(4) (2.15)	2.208(4) (2.22: Mn^{2+}) (2.05: Mn^{3+})
$T2$–O4	2.047(2) (2.12)	2.045(3) (2.14)	2.045(4) (2.15)	2.104(5) (2.22: Mn^{2+}) (2.05: Mn^{3+})
Mo–O1	2.0263(18)	2.022(3)	2.027(4)	2.035(4)
Mo–O2	2.1421(14)	2.1389(19)	2.145(3)	2.151(3)
Mo–O3	2.0761(11)	2.0782(14)	2.085(2)	2.074(3)
Mo–O4	1.9522(15)	1.952(2)	1.957(3)	1.958(4)
Mo–Mo	2.5271(2)	2.5274(4)	2.5325(6)	2.5391(6)

Table 3
Bond valences of the T and Mo ions in $T_2Mo_3O_8$.

	$Mg_2Mo_3O_8$	$Co_2Mo_3O_8$	$Zn_2Mo_3O_8$	$Mn_2Mo_3O_8$
T ions	Mg^{2+}	Co^{2+}	Zn^{2+}	Mn^{2+}
R_0 (Å)	1.693	1.692	1.704	1.790
V_{T1}	+1.977	+1.933	+2.008	+2.109
V_{T2}	+2.148	+2.094	+2.147	+2.253
Mo	+4.054	+4.060	+3.999	+4.007

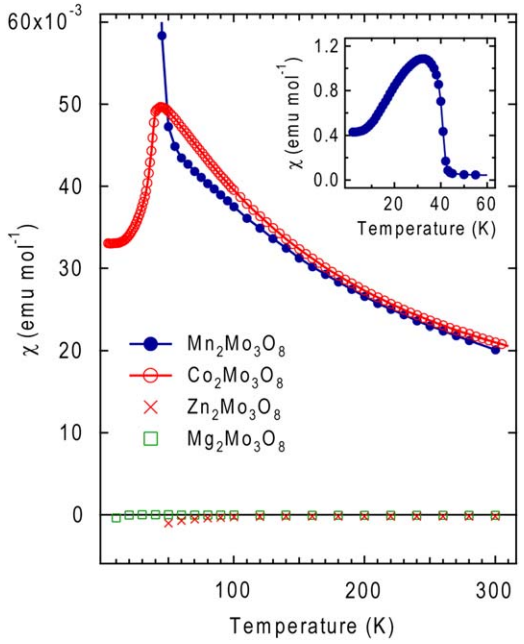

Fig. 3. Magnetic susceptibilities of $T_2Mo_3O_8$ as functions of temperature. Inset shows a plot of the magnetic susceptibility of $Mn_2Mo_3O_8$ below 60 K.

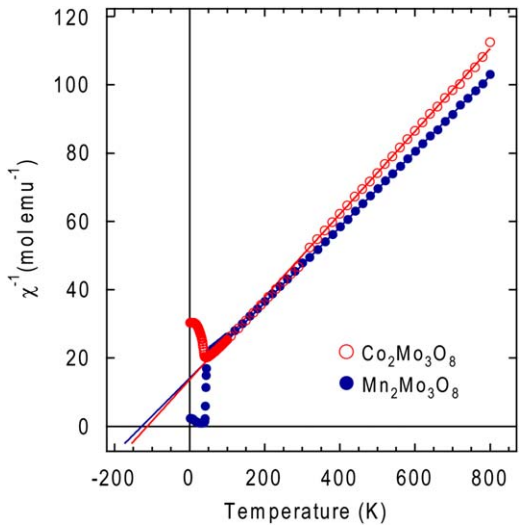

Fig. 4. Reciprocal magnetic susceptibilities of $T_2Mo_3O_8$ (T=Co and Mn) as functions of temperature.

and $Zn_2Mo_3O_8$ is consistent with the premise that the valences of the T ions and Mo_3 (T=Mg and Zn) are +2 and +12, respectively. The non-magnetic, closed-shell Mo^{12+} does not contribute to the net magnetization [19].

The red open circles represent the magnetic susceptibility of $Co_2Mo_3O_8$ (χ_{Co}). Unlike either χ_{Mg} or χ_{Zn}, χ_{Co} increases monotonously with decreasing the temperature from 300 to 40 K. χ_{Co} shows a steep decrease at 40 K, which is assigned to an antiferromagnetic ordering of the local moments of Co [21,22]. The blue closed circles represent the magnetic susceptibility of $Mn_2Mo_3O_8$ (χ_{Mn}). Similar to χ_{Co}, χ_{Mn} monotonously increases with a decrease in temperature from 300 to 45 K. χ_{Mn} steeply rises at a transition temperature of 43 K and shows a peak at 35 K. The inset shows χ_{Mn} near the transition temperature. The χ_{Mn} at 35 K is nearly 30 times larger than that at 45 K. The anomaly of χ_{Mn} at 43 K is attributed to a ferrimagnetic ordering of the local moments of Mn [21–24].

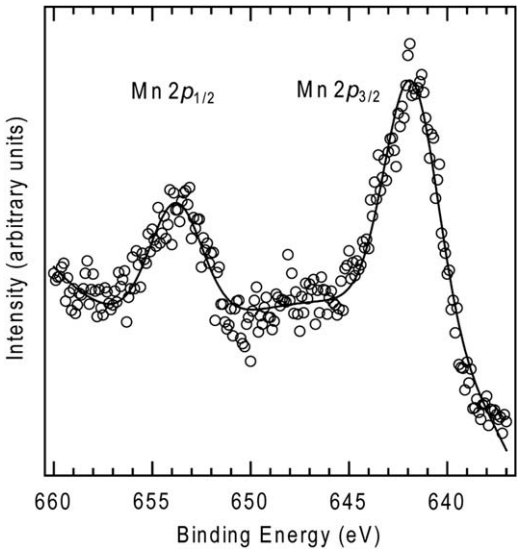

Fig. 5. XPS spectrum of the Mn 2p shells for $Mn_2Mo_3O_8$.

Table 4
XPS binding energies for $Mn_2Mo_3O_8$ and the reference specimens.

Compound	Mn $2p_{3/2}$ (eV)	Mn $2p_{1/2}$ (eV)	Δ[a] (eV)
$Mn_2Mo_3O_8$	641.9 ± 0.2	653.8 ± 0.2	11.9
MnO	641.9 ± 0.2	653.9 ± 0.2	12.0
Mn_2O_3	642.3 ± 0.2	653.8 ± 0.2	11.5
MnO_2	642.8 ± 0.2	654.3 ± 0.2	11.5

[a] Δ: spin–orbit splitting.

The reciprocal magnetic susceptibilities of $Co_2Mo_3O_8$ and $Mn_2Mo_3O_8$, $(\chi_{Co})^{-1}$ and $(\chi_{Mn})^{-1}$, respectively, are plotted in Fig. 4 as functions of temperature. Both $(\chi_{Co})^{-1}$ and $(\chi_{Mn})^{-1}$ show a linear dependence on temperature from 300 to 800 K. The effective magnetic moments, μ_{eff}, of $Co_2Mo_3O_8$ and $Mn_2Mo_3O_8$ are calculated on the basis of Curie–Weiss analysis in the temperature range of 400 to 800 K. The μ_{eff} of $Co_2Mo_3O_8$ is evaluated to be 4.0 μ_B/Co, which is consistent with the values reported in the literature, 4.34 μ_B/Co [11] and/or 3.9 μ_B/Co [22]. The μ_{eff} evaluated by this work, 4.0 μ_B/Co, is also consistent with the value expected for the high-spin state of Co^{2+} ions, 3.873 μ_B/Co^{2+} (S=3/2). It is reasonable to conclude that the valence of the Co ions in $Co_2Mo_3O_8$ is +2. As in the cases of $Mg_2Mo_3O_8$ and $Zn_2Mo_3O_8$, the closed-shell Mo_3^{12+} in $Co_2Mo_3O_8$ does not contribute to the net magnetization of the compound.

The μ_{eff} of $Mn_2Mo_3O_8$ is evaluated to be 4.36 μ_B/Mn, which shows a deviation from the literature values evaluated by Curie–Weiss analysis at temperatures lower than 300 K, 4.93 μ_B/Mn [11], 6.1 μ_B/Mn [21], 5.9 μ_B/Mn [22] or 6.40 μ_B/Mn [24]. It is worth noting that the evaluated μ_{eff} for $Mn_2Mo_3O_8$, 4.36 μ_B/Mn, is consistent with the average magnetic moment determined by neutron diffraction, 4.3 ± 0.3 μ_B/Mn [21]. The μ_{eff} for $Mn_2Mo_3O_8$ is much smaller than 5.916 μ_B/Mn^{2+} (S=5/2) and consistent with either 4.899 μ_B/Mn^{3+} (S=2) or 3.873 μ_B/Mn^{4+} (S=3/2). The average valence of the Mn1 and Mn2 ions in $Mn_2Mo_3O_8$ is close to either +3 or +4.

Fig. 5 shows an XPS spectrum for $Mn_2Mo_3O_8$ in the Mn 2p region. Two peaks at 641.9 ± 0.2 and 653.8 ± 0.2 eV are assigned to the Mn $2p_{3/2}$ and $2p_{1/2}$ emissions, respectively. The slight convex at around 648 eV could be attributed to a shake-up satellite of the Mn 2p emissions.

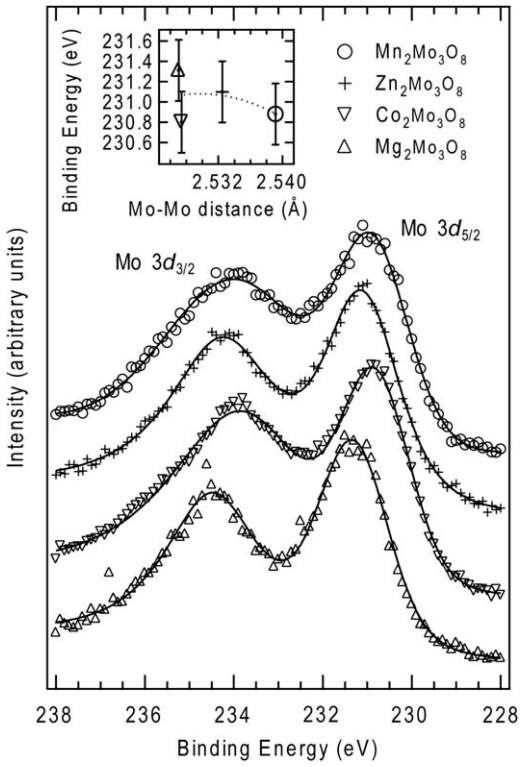

Fig. 6. XPS spectra of the Mo 3*d* shells for $T_2Mo_3O_8$. Inset shows the relation between the Mo–Mo distances and the Mo $3d_{5/2}$ binding energies.

The Mn $2p_{3/2}/2p_{1/2}$ binding energies for $Mn_2Mo_3O_8$ are listed in Table 4, together with the values for the reference specimens. The values for the reference specimens are consistent with those reported in the literature [27,28]. The Mn $2p_{3/2}/2p_{1/2}$ binding energies for $Mn_2Mo_3O_8$ are consistent with those for MnO and/or Mn_2O_3 within experimental errors. In contrast, the Mn $2p_{3/2}/2p_{1/2}$ binding energies for MnO_2 show finite deviation from those for $Mn_2Mo_3O_8$. The valence of the Mn ions in $Mn_2Mo_3O_8$ lies, therefore, between +2 and +3. Taking into account the results of XRD, the magnetization measurements and XPS, we conclude that the Mn1 and Mn2 ions in $Mn_2Mo_3O_8$ adopt different valences, +2 and $2+\delta$ ($\delta > 0$), respectively, whereas the value of the *T* ions in the other $T_2Mo_3O_8$ (*T*=Mg, Zn or Co) is +2 regardless of sites. In terms of electric neutrality of the compound, the formal valence of the Mo_3 in $Mn_2Mo_3O_8$ is determined as $12-\delta$.

Fig. 6 shows XPS spectra for $T_2Mo_3O_8$ in the Mo 3*d* region. The peaks near 231 and 234 eV are assigned to the Mo $3d_{5/2}$ and $3d_{3/2}$ emissions, respectively. The Mo $3d_{5/2}/3d_{3/2}$ binding energies show a dependence on the kind of the *T* ions. The inset shows the Mo $3d_{5/2}$ binding energies as a function of the Mo–Mo distance (see Table 2) for $T_2Mo_3O_8$. The Mo $3d_{5/2}$ binding energies tend to decrease in the order of *T*=Mg, Co, Zn and Mn, along with an increase in the Mo–Mo distance. Both the lowering of Mo $3d_{5/2}$ binding energy and the large Mo–Mo distance for $Mn_2Mo_3O_8$ are consistent with the existence of excessive electrons on the $Mo_3^{12-\delta}$ in $Mn_2Mo_3O_8$. Indeed, Torardi et al. have shown that the Mo–Mo distance of a Mo_3^{11+} in $LiZn_2Mo_3^{11+}O_8$ is lager than that of a Mo_3^{12+} in $Zn_2Mo_3^{12+}O_8$, owing to excessive electrons on Mo_3^{11+} [10].

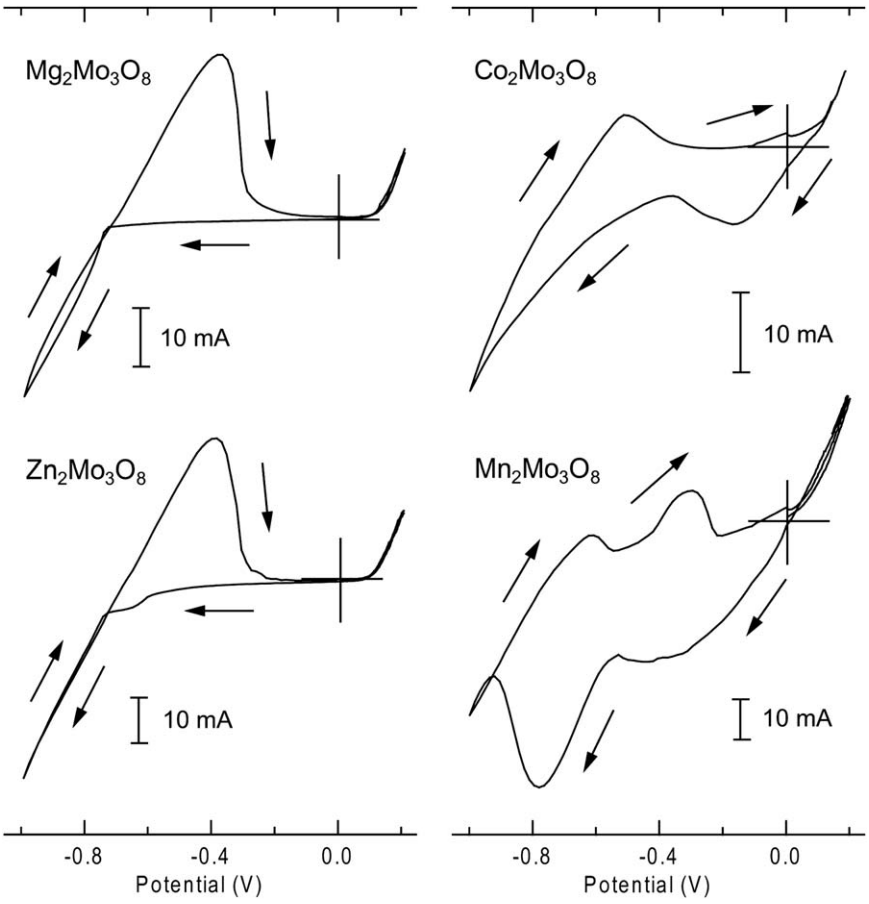

Fig. 7. Cyclic voltammetry (CV) profiles for $T_2Mo_3O_8$.

Fig. 7 shows the cyclic voltammetry (CV) profiles for $T_2Mo_3O_8$. The ionic current for $Mg_2Mo_3O_8$ (I_{Mg}) monotonously decreases on the cathodic sweep from +0.20 to −0.70 V. The sharp drop of I_{Mg} at −0.75 V corresponds to the reduction of $MgMo^{6+}O_4$ to precipitate $Mg_2Mo_3^{4+}O_8$ crystals. On the anodic sweep from −1.0 V, the I_{Mg} shows a peak at −0.39 V. This peak is attributed to the oxidation of the Mo^{4+} ions in $Mg_2Mo_3^{4+}O_8$ to Mo^{6+} ions ($Mo^{4+} \rightarrow Mo^{6+}$). The ionic current for $Zn_2Mo_3O_8$ (I_{Zn}) shows a potential dependence similar to that of the I_{Mg}. The peak of I_{Zn} at −0.40 V on the anodic sweep corresponds to the $Mo^{4+} \rightarrow Mo^{6+}$. The ionic current for $Co_2Mo_3O_8$ (I_{Co}) shows a valley at −0.18 V and a peak at −0.39 V on the cathodic sweep. The peak of I_{Co} at −0.52 V on the anodic sweep corresponds to the $Mo^{4+} \rightarrow Mo^{6+}$.

The ionic current for $Mn_2Mo_3O_8$ (I_{Mn}) shows two peaks at −0.61 and −0.30 V on the anodic sweep, unlike the single peaks observed for the other I_T (T=Mg, Zn or Co). The peak of I_{Mn} at −0.61 V can be attributed to the oxidation of the $Mo_3^{12-\delta}$ clusters in $Mn_2Mo_3O_8$ to Mo_3^{12+} ($Mo_3^{12-\delta} \rightarrow Mo_3^{12+}$). The peak of I_{Mn} at −0.30 V corresponds to the $Mo^{4+} \rightarrow Mo^{6+}$. The $Mo_3^{12-\delta} \rightarrow Mo_3^{12+}$ is associated with a transfer of less than one electron per one Mo_3 cluster, whereas the $Mo^{4+} \rightarrow Mo^{6+}$ is associated with a transfer of two electrons per one Mo ion. The peak of I_{Mn} corresponding to the $Mo_3^{12-\delta} \rightarrow Mo_3^{12+}$ is, indeed, smaller than that corresponding to the $Mo^{4+} \rightarrow Mo^{6+}$.

Cotton showed that Mo_3^{12+} possesses a non-bonding (or weakly anti-bonding) lowest unoccupied molecular orbital with the A_1 symmetry (A_1-LUMO) [7]. Excessive electrons of $Mo_3^{12-\delta}$ relative to Mo_3^{12+} are most likely accepted by the A_1-LUMO to become unpaired electrons. The unpaired electron does not participate in the chemical bonding among any of the constituent atoms of $Mn_2Mo_3O_8$. $Mn_2Mo_3O_8$ has potential as a Lewis-base catalyst since the unpaired electrons on the $Mo_3^{12-\delta}$ might act as an effective catalysis center.

4. Conclusions

In conclusion, we have demonstrated that the Mo_3 cluster in $Mn_2Mo_3O_8$ adopts an anomalous valence of $12-\delta$ ($\delta > 0$), unlike the Mo_3^{12+} clusters that are usually recognized for the known Mo_3-containing compounds. The $Mo_3^{12-\delta}$ in $Mn_2Mo_3O_8$ possesses excessive electrons relative to Mo_3^{12+}. $Mn_2Mo_3O_8$ is worthy of further research as a Lewis-base catalyst due to the unpaired electrons on the $Mo_3^{12-\delta}$.

Supporting information

X-ray crystallographic data in CIF format for $T_2Mo_3O_8$ (T=Mg, Co, Zn and Mn), as well as a table that represents the refined positional parameters (S1).

Acknowledgments

This work was supported by the Ministry of Education, Culture, Sports, Science and Technology (MEXT) and the Japan Society for the Promotion of Science (JSPS) through Grant-in-Aid 19560845.

Appendix A. Supplementary material

Supplementary data associated with this article can be found in the online version at doi:10.1016/j.jssc.2009.11.024.

References

[1] W.L. Gladfelter, K.J. Roesselet, in: D.F. Shriver, H.D. Kaesz, R.D. Adams (Eds.), The Chemistry of Metal Cluster Complexes, VCH, New York, 1990.
[2] J.A. Cabeza, J.M. Fernández-Colinas, A. Llamazares, V. Riera, Organometallics 13 (1994) 4352–4359.
[3] S. Hanada, T. Ishida, Y. Motoyama, H. Nagashima, J. Org. Chem. 72 (2007) 7551–7559.
[4] M. Feliz, E. Guillamón, R. Llusar, C. Vicent, S.E. Stiriba, J. Pérez-Prieto, M. Barberis, Chem. Eur. J. 12 (2006) 1486–1492.
[5] E. Guillamón, R. Llusar, J. Pérez-Prieto, S.-E. Stiriba, J. Organomet. Chem. 693 (2008) 1723–1727.
[6] F.A. Cotton, T.E. Haas, Inorg. Chem. 3 (1964) 10–17.
[7] F.A. Cotton, Inorg. Chem. 3 (1964) 1217–1220.
[8] J. Mizutani, H. Imoto, T. Saito, J. Clust. Science 6 (1995) 523–532.
[9] C.C. Torardi, R.E. McCarley, J. Solid State Chem. 37 (1981) 393–397.
[10] C.C. Torardi, R.E. McCarley, Inorg. Chem. 37 (1985) 476–481.
[11] W.H. McCarroll, L. Katz, R. Ward, J. Amer. Chem. Soc. 79 (1957) 5410–5414.
[12] G.B. Ansell, L. Katz, Acta Cryst. 121 (1966) 482–485.
[13] J. Cuny, P. Gougeon, P. Gall, Acta Cryst. E 65 (2009) i51.
[14] Y. Le Page, P. Strobel, Acta Cryst. B 38 (1982) 1265–1267.
[15] Y. Kanazawa, A. Sasaki, Acta Cryst. C 42 (1986) 9–11.
[16] R. Knorr, U. Müller, Z. Anorg. Allg. Chem. 621 (1995) 541–545.
[17] P. Strobel, Y. Le Page, J. Cryst. Growth 61 (1983) 329–338.
[18] W.H. McCarroll, C. Darling, G. Jakubicki, J. Solid State Chem. 48 (1983) 189–195.
[19] F. Varret, H. Czeskleba, F. Hartmann-bourtron, P. Imbert, J. Physique 33 (1972) 549–564.
[20] P. Strobel, Y. Le Page, S.P. McAlister, J. Solid State Chem. 42 (1982) 242–250.
[21] D. Bertrand, H. Kerner-Czeskleba, J. Physique 36 (1975) 379–390.
[22] S.P. McAlister, P. Strobel, J. Mag. Mag. Mater. 30 (1983) 340–348.
[23] S.P. McAlister, J. Appl. Phys. 55 (1984) 2343–2345.
[24] B. Lippold, J. Hermann, W. Reichelt, H. Oppermann, Phys. Stat. Sol. 121 (1990) K91–K95.
[25] R.D. Shannon, C.T. Prewitt, Acta Cryst. B 25 (1969) 925–946.
[26] I.D. Brown, The Chemical Bond in Inorganic Chemistry: The Bond Valence Model (International Union of Crystallography Monographs on Crystallography), Oxford University Press, Oxford, 2002.
[27] B.J. Tan, K.J. Klabunde, P.M.A. Sherwood, J. Amer. Chem. Soc. 113 (1991) 855–861.
[28] J.C. Carver, G.K. Schweitzer, T.A. Carlson, J. Phys. Chem. 57 (1972) 973–982.